Magnetic structures and magnetocaloric effect in RVO_4 (R = Gd, Nd)

E. Palacios,[1,2] M. Evangelisti,[1,2] R. Sáez-Puche,[3] A. J. Dos Santos-García,[4] F. Fernández-Martínez,[4] C. Cascales,[5] M. Castro,[1,6] R. Burriel,[1,2] O. Fabelo,[7] and J. A. Rodríguez-Velamazán[7]

[1]*Instituto de Ciencia de Materiales de Aragón (ICMA), CSIC, Universidad de Zaragoza, 50009 Zaragoza, Spain*
[2]*Departamento de Física de la Materia Condensada, Universidad de Zaragoza, 50009 Zaragoza, Spain*
[3]*Departamento de Química Inorgánica, Universidad Complutense de Madrid, 28040 Madrid, Spain*
[4]*Departamento de Ingeniería Mecánica, Química y Diseño Industrial, ETSIDI, Universidad Politécnica de Madrid, 28012 Madrid, Spain*
[5]*Instituto de Ciencia de Materiales de Madrid, CSIC, Campus de Cantoblanco, 28049 Madrid, Spain*
[6]*Departamento de Ciencia y Tecnología de Materiales y Fluidos, Universidad de Zaragoza, 50018 Zaragoza, Spain*
[7]*Institut Laue-Langevin, 38042 Grenoble Cedex 9, France*

(Received 16 March 2018; revised manuscript received 16 May 2018; published 1 June 2018)

We report the magnetic properties and magnetic structure of the zircon-type compound $GdVO_4$, together with the magnetic structure of the isostructural $NdVO_4$. At $T \simeq 2.5$ K, $GdVO_4$ undergoes a phase transition to antiferromagnetic G_z, driven mainly by the exchange interactions, while the magnetic anisotropy and dipolar interactions are minor contributions. Near the liquid-helium boiling temperature, the magnetocaloric effect of $GdVO_4$ is nearly as large as that of the structurally closely related $GdPO_4$. It is noteworthy that $GdVO_4$ has been recently proposed as a good passive regenerator in Gifford-McMahon cryocoolers, since adding a magnetization-demagnetization stage to the cryocooler refrigeration cycle would increase its efficiency for liquefying helium. $NdVO_4$ is a canted G_z-type antiferromagnet and shows enhancement of the magnetic reflections in neutron diffraction below ca. 500 mK, due to the polarization of the Nd nuclei by the hyperfine field.

DOI: 10.1103/PhysRevB.97.214401

I. INTRODUCTION

Adiabatic demagnetization was the first procedure used to attain temperatures close to absolute zero. The best-suited materials for this task are inorganic salts with a very low magnetic density, to prevent magnetic ordering to occur. Using demagnetization from low applied fields or at relatively high temperatures, the refrigeration capacity of a paramagnet is roughly inversely proportional to the square of temperature, therefore these refrigerant materials are only relevant below 1 K. Magnetic refrigeration lost popularity some years ago because of the development of ^{3}He/^{4}He dilution refrigerators. However, that technique is very efficient thermodynamically, leading to an energy saving that is of paramount importance for large-scale applications. Such an efficiency has been further maximized by developing refrigeration procedures based on the Carnot cycle [1]. Slowly but constantly, magnetic refrigeration is regaining interest as the physical principle of choice for, e.g., liquifying helium and hydrogen, cooling in space-borne missions, and other applications [2]. Besides, several companies are currently operating in the market of adiabatic demagnetization refrigerators. A recent and extensive review of foundations, materials, and systems for magnetic refrigeration can be seen in Ref. [3] and specifically for cryogenic purposes in Ref. [4].

Magnetic refrigeration exploits the magnetocaloric effect (MCE), whose main parameters are the adiabatic temperature increment ΔT_{ad} and the isothermal entropy increment ΔS_T (<0, usually) following any applied field increment ΔB. Moreover, prototypes of magnetic refrigerators for liquefying helium, hydrogen, or other natural gases have been proposed [5–7]. In the $4 \lesssim T \lesssim 50$ K temperature range, typical paramagnetic salts are no longer very efficient and other types of materials have been explored for achieving a stronger MCE [1]. The most evident among them are ferromagnets with the Curie temperature in the working temperature range, and $Er(Co_{1-x}Ni_x)_2$ with $T_C = 13$–35 K, depending on x, represents an outstanding example. This alloy can show a large MCE, e.g., $\Delta S_T \simeq -10$ J kg^{-1} K^{-1} for $\Delta B = 0$–5 T, though only for a narrow temperature range near T_C. Recently, the polarization of a rare-earth atom by the exchange field produced by a transition metal has revealed itself as an interesting mechanism to increase the MCE over a much wider T span, as reported for $GdCrO_4$ [8,9].

A different approach consists of combining a high magnetic density with a frustrating spin spatial arrangement, which ultimately inhibits the magnetic ordering. The most studied example is $Gd_3Ga_5O_{12}$ (gadolinium gallium garnet, abbreviated as GGG) that shows $-\Delta S_T > 25$ J kg^{-1} K^{-1} below 10 K, for $\Delta B = 0$–8 T. [1] Recently, we reported the interesting $GdPO_4$ that, for $\Delta B = 0$–7 T, shows $-\Delta S_T > 30$ J kg^{-1} K^{-1} between 1 and 10 K and a maximum $-\Delta S_{T,max} = 63$ J kg^{-1} K^{-1} at $T = 2.1$ K [10]. This compound has the frustrating monazite structure and is an electrical insulator, which prevents the Ruderman-Kittel-Kasuya-Yosida (RKKY) mechanism for exchange interactions. In competition with the weak magnetic anisotropy, dipole-dipole interactions promote spin ordering below $T_N = 0.77$ K in a noncollinear arrangement.

Hereafter, we focus on RVO_4, where R is either Gd or Nd. Gadolinium orthovanadate is somewhat similar to $GdCrO_4$ and $GdPO_4$ alloys previously studied [8–10]. However, it significantly differs from $GdPO_4$ since $GdVO_4$ has a more symmetric, nonfrustrating, zircon ($ZrSiO_4$-type) structure, in

which each Gd^{3+} ion has four nearest neighbors of the same type at 3.93 Å, forming a distorted diamond lattice shown below. Consequently, $GdVO_4$ orders at a relatively higher temperature $T_N = 2.5$ K, more than three times higher than for $GdPO_4$, and which is clearly too high to be produced by the dipolar interaction. The present study on $GdVO_4$ also sheds light on the analysis of the $GdCrO_4$ data reported in Ref. [8]. There, the Gd-Gd exchange interaction was neglected because of the much stronger and dominating Gd-Cr and Cr-Cr interactions. From $GdVO_4$, where Cr is replaced by the nonmagnetic V, we now obtain an estimate of the strength of the Gd-Gd exchange interaction. Its $(\partial T/\partial B)_{\rm ad}$, deduced by an interesting ac technique, was reported in 1991 [11] and applied to the determination of the magnetic phase diagram, in a single crystal with the field parallel to the c axis. More importantly, the magnetic properties of $GdVO_4$ have been reported very recently [12]. Nevertheless the thermal properties under magnetic field and its magnetic structure have not been studied, even though these properties are technologically relevant, as proven by the fact that this material is already proposed as a good passive regenerator in cryocoolers based on the Gifford-McMahon (GM) cycle. [13] The efficiency of the GM cycle can be enhanced by replacing the passive regenerator by an active magnetic regenerator and by including magnetization and demagnetization steps in the cycle [1,15].

Also $NdVO_4$ has the zircon structure and, from magnetic susceptibility, it was deduced that it orders magnetically at $T_N = 820$ mK, possibly in a canted antiferromagnetic structure [14,16]. The ac susceptibility for the applied field along the crystal a direction was reported to show a peak at 840 mK [16,17]. This compound offers the possibility to study the polarization of the Nd nucleus exerted by the electronic magnetic field. Although the nuclear magnetic moment is by far too small to be observed by neutron diffraction, nuclear polarization is seen to modify the nuclear scattering length, which is an average over the nuclear spin states [18]. The effect is particularly strong for ^{143}Nd and ^{145}Nd, amounting to 20.47% of natural Nd, due to the large incoherent scattering cross sections of both isotopes. Several studies on the polarization of the Nd nucleus were reported for a number of compounds already in the 1990s. However, conclusive results were not always obtained either because the experiments were performed on powdered samples [19,20] or twinned crystals [21,22] or on crystals whose magnetic structure could not be solved [23]. For $NdFeO_3$, the results are very much affected by the strong exchange field of the Fe^{3+} ions, making difficult the analysis on the polarization of the Nd nuclei.

Below, we investigate the heat capacity (Sec. II) and the magnetocaloric effect (Sec. III) of $GdVO_4$ between 300 mK and 30 K, and the magnetic structures (Sec. IV) of $GdVO_4$ and $NdVO_4$, as determined by neutron diffraction experiments, carried out between ca. 60 mK and 4 K on single crystals.

II. HEAT CAPACITY OF $GdVO_4$

The heat capacity of $GdVO_4$, C_B, has been measured on a pressed powder wafer-shaped sample of 3.54 mg and about 3 mm diameter by the standard relaxation method in a Quantum Design Physical Properties Measurement System (PPMS) setup, at constant magnetic fields up to $B = 7$ T.

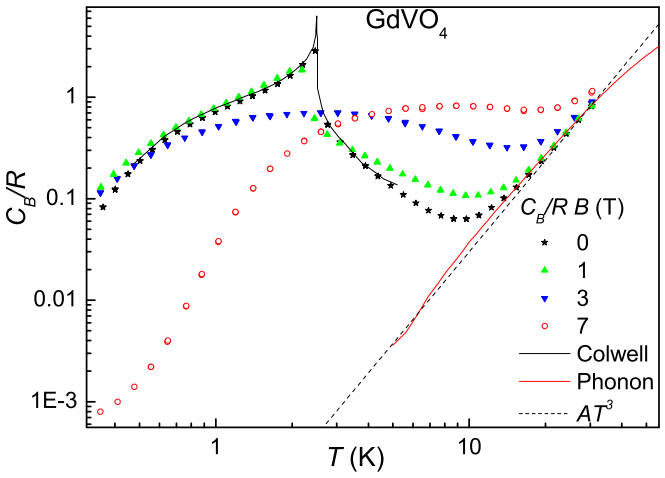

FIG. 1. Heat capacity at constant field, normalized to the gas constant, C_B/R, vs temperature at several values of the applied magnetic fields for $GdVO_4$, in a double-log scale. Black continuous line was obtained from Ref. [25]. Red line is the phonon contribution, estimated as C of $ZrSiO_4$ for $T \times f$, where $f = 1.6$ (see main text). Black dashed line corresponds to the simple estimation $C_{\rm ph}/R \simeq AT^3$ (see main text). Numerical data are accessible in the Supplemental Material [26].

The results are plotted in a double log scale in Fig. 1. For $B = 0$, they agree very well with those reported in Ref. [24], also plotted in Fig. 1 of Ref. [25]. There is a peak at $T_N = 2.50$ K attributable, according to susceptibility data [16,17], to an antiferromagnetic ordering. The phonon contribution, $C_{\rm ph}$, can be estimated from the isostructural nonmagnetic compound $ZrSiO_4$, applying a temperature scale factor of $f = 1.6[C_{\rm ph}(GdVO_4, T) \simeq C_{\rm ph}(ZrSiO_4, T \times f)]$, due mainly to the different molar mass but also to different bonding of both compounds. The so-obtained phonon contribution fits well, below 30 K, to a Debye $C_{\rm ph}/R \simeq AT^3$ law, with $A = 2.9 \times 10^{-5}$ K^{-3}. In any case, $C_{\rm ph}$ is only a small contribution over the peak T range. The total entropy can be computed from the thermodynamic relation

$$S(T,B) = S(T_0,B) + \int_{T_0}^{T} \frac{C_B(T',B)}{T'} dT', \qquad (1)$$

from which we obtain the magnetic contribution to the entropy, $S_m(T,B) = S(T,B) - AT^3/3$. The most direct way of computing Eq. (1) is to take $T_0 = 0$, since $S(T_0 = 0, B) = 0$, according to the Third Law of Thermodynamics. Ideally, low enough temperatures should be reached in order to do a proper extrapolation of the experimental data down to $T \to 0$. However, this is not always feasible and, in the present case, the extrapolation of the entropy from ca. 300 mK is obvious only for the data collected at high fields. We did so for $B = 7$ T. For other field values, we have adopted a different procedure, as follows.

The highest experimental temperature, $T \approx 30$ K, is more than ten times T_N. Therefore, the magnetocaloric properties of $GdVO_4$ at such a high temperature can be confidently estimated from mean-field theory for a simple two sublattices antiferromagnet with spin $s = 7/2$. The magnetic entropy for a pure paramagnet in an external field B is exactly

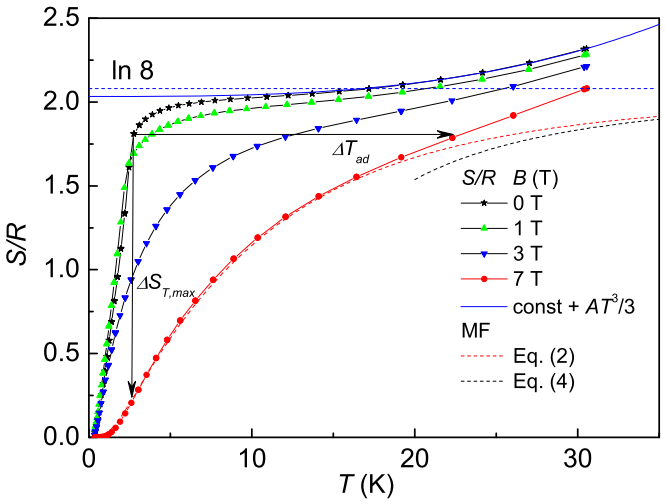

FIG. 2. Isofield curves in an S/T diagram obtained by integration of C_B/T. Red dashed line: mean field (MF) approximation for the magnetic contribution at $B = 7$ T and $T > T_N$, Eq. (2). Black dashed line: High T approximation, Eq. (4). Blue dashed line: Expected value of the molar magnetic entropy for $s = 7/2$ at $T \to \infty$. Continuous blue line: Fit of the experimental entropy, with $S = 2.04 + AT^3/3$ for $B = 0$ in the high-T range. The vertical arrow depicts how to compute ΔS_T, for the largest applied field change ΔB from 0 to 7 T. The horizontal arrow shows the computation of $\Delta T_{\rm ad}$ for the same initial temperature and field variation. Numerical data are accessible in the Supplemental Material [26].

given by [1,27]

$$\frac{S_m}{R} = \ln \frac{\sinh[x(2s+1)/(2s)]}{\sinh[x/(2s)]} - x B_s(x), \qquad (2)$$

where $B_s(x)$ is the Brillouin function for spin s and $x = g\mu_B s B/k_B T$.

For $x << 1$, $B_s(x) \simeq x(s+1)/(3s)$ and the first term in Eq. (2) is $\ln(2s+1)$. Therefore the above expression can be approximated by

$$\frac{S_m}{R} = \ln(2s+1) - \frac{(s+1)x^2}{3s} = \ln(2s+1) - \frac{1}{2}\frac{C_s B^2}{RT^2}, \qquad (3)$$

with the Curie constant for spin s, $C_s = N_A \mu_B^2 g^2 s(s+1)/3k_B$, N_A being the Avogadro's constant.

For an antiferromagnetic substance, within the mean-field approximation, and for $T \gg T_N$, the same expression (3) can be used, replacing the external field B by the mean field $B_{\rm mf} = BT/(T+\theta)$, which gives, when $T >> T_N$,

$$S_m/R \simeq \ln(2s+1) - \frac{1}{2}\frac{C_s B^2}{R(T+\theta)^2}. \qquad (4)$$

The value $\theta = 0.7$ K has been adjusted to get a good fit of Eq. (2), between 5 and 10 K, with the experimental absolute entropy determined for $B = 7$ T by integration of C_B/T. In this range the phonon contribution is negligible and the mean-field approach very precise. Figure 2 shows the experimental entropy at 7 T along with the magnetic entropy computed with Eq. (2) and the high-temperature approximation, Eq. (4). Finally the high-temperature approximation is used to determine the entropy differences for 0, 1, and 3 T, with respect to the absolute entropy for 7 T, at the highest temperature, $T_0 = 30$ K. These values allow determining the entropy at any other temperatures via Eq. (1).

The so-obtained isofield curves extrapolate indeed to zero for $T \to 0$, in an S-T diagram, Fig. 2. The magnetic entropy, computed as the difference of the total entropy minus the phonon contribution at 30 K, $S_m(T \to \infty)/R = 2.04 \pm 0.05$ agrees well with the expected value for a spin $s = 7/2$, $\ln(2s+1) = 2.08$.

III. MAGNETOCALORIC EFFECT OF $GdVO_4$

The characteristic magnetocaloric values of ΔS_T and $\Delta T_{\rm ad}$ can be deduced from the heat capacity data. According to Eq. (1), we have

$$\Delta S_T \equiv S(T,B) - S(T,0) = S(T_0,B) - S(T_0,B=0) + \int_{T_0}^{T} \frac{C_B(T',B) - C_B(T',0)}{T'} dT'. \qquad (5)$$

Furthermore, from $S(T,B)$ the temperature differences can be computed for any given entropy,

$$\Delta T_{\rm ad} = T(S,B) - T(S,B=0), \qquad (6)$$

as sketched in Fig. 2. As explained above, ΔS_T has been estimated at $T_0 = 30$ K, where it is small anyway, by the mean-field approximation for every field and deduced via Eq. (5) at other temperatures. Figure 2 shows graphically these procedures, while Fig. 3 shows the so-obtained results for ΔS_T (top panel) and $\Delta T_{\rm ad}$ (bottom panel). It can be seen that $-\Delta S_T$ reaches the maximum value of 48 J kg^{-1} K^{-1} at $T \simeq 3$ K, which is somewhat lower than for $GdPO_4$, due to the relatively stronger antiferromagnetic correlations in $GdVO_4$, and also due to the smaller molar mass of the orthophosphate. Nonetheless, the MCE of $GdVO_4$ is very high, overcoming that of the reference magnetic refrigerant GGG at any temperature above T_N (see Fig. 3; note that the difference is even larger than depicted since the GGG data shown in the figure are collected for $\Delta B = 8$ T). The reported data [28] for $GdVO_4$, with $\Delta B = 5$ T, agree with the present determination except at higher temperatures, when those values nearly overlap with ours for 3 T. In any case, in this temperature range $|\Delta S_T|$ is small and has large relative errors. The values of $\Delta T_{\rm ad}$ for $GdVO_4$ are similar to those of $GdPO_4$ for $T > 5$ K. We finally mention that recent data of ΔS_T deduced from isothermal magnetization [12] via the Maxwell relation agree with the present ones, $-\Delta S_{T,\max} = 41.1$ J kg^{-1} K^{-1} at $T \simeq 3$ K for $\Delta B = 5$ T, higher than that reported in Ref. [28], and they also agree with the data for $\Delta T_{\rm ad}$, $\Delta T_{\rm ad,max} = 18$ K at $T \simeq 5$ K for the same applied field change.

IV. NEUTRON DIFFRACTION

A. Experimental details

The neutron diffraction experiments on $GdVO_4$ and $NdVO_4$ single crystals were performed at the D9 instrument of the Institute Laue-Langevin (Grenoble). The experiments were carried out between ca. 60 mK and 8 K to determine the magnetic structures and to collect data on the nuclear contribution in the magnetically disordered phase. This temperature range

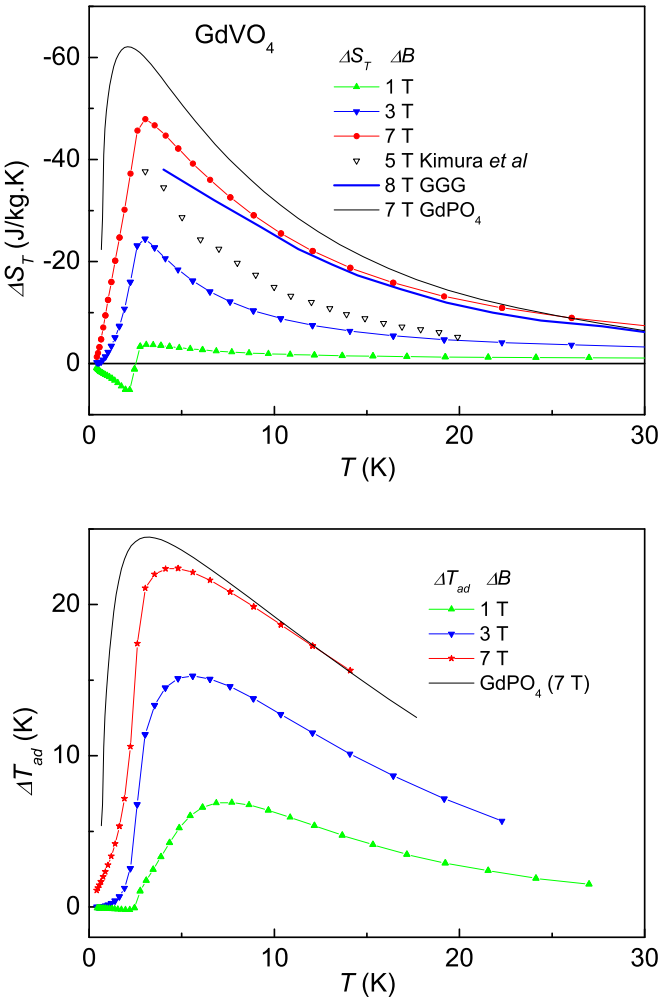

FIG. 3. Magnetocaloric effect of $GdVO_4$ for magnetic field changes from 0 to 1, 3, and 7 T, respectively, as obtained from heat capacity data. Top panel: Isothermal entropy change $-\Delta S_T$. Data for 5 T from Kimura *et al.* [28] and for $GdPO_4$ (Ref. [10]) and GGG (Ref. [1]) are also included for comparison. Bottom panel: Adiabatic temperature change ΔT_{ad}. Numerical data accessible in the Supplemental Material [26].

was explored using a ^{3}He/^{4}He dilution cryostat. For both experiments, a single-crystal sample with needle shape was glued having the longest axis (c crystal axis) oriented vertically. This setup imposes the Weissenberg normal beam geometry, when the cryostat and detector can be turned around z and the detector has also a short range of motion away of the horizontal plane. Considering the cell dimensions of the crystals, the accessible reflections are indexed as (h,k,l) with $l = 0,1$, for the wavelengths $\lambda = 0.5130$ Å and 0.8347 Å. These values were refined in an independent experiment, hereafter shortened as 0.5 and 0.8 Å, respectively.

The $GdVO_4$ single crystal was a needle of $0.25 \times 0.25 \times 4$ mm^3, having the c axis oriented along its length. Note that too wide a needle is not adequate due to the huge absorption of natural Gd for thermal neutrons. Although the use of hot neutrons, of shorter wavelengths, reduces the absorption to bearable values, the single-crystal sample should be thin and its diameter should allow giving a correct balance between intensity and absorption. In general, for a given crystal volume, the needle shape habit has lower diffracted/absorbed intensity ratio than the platelet habit. The absorption was corrected assuming a cylindrical crystal, using the parameters given in the International Tables for Crystallography (ITC) [29]. For the available crystal and $\lambda = 0.8$ Å the absorption is roughly ten times higher than for $\lambda = 0.5$ Å, but also the neutron flux is about four times higher and, therefore, the observed count number could be observed for both wavelengths with similar collection times. The higher wavelength allows scanning the low-angle reflections (1,0,0) and (0,1,0), to check if they are actually absent. Besides, some reflections were observed as strong with $\lambda = 0.5$ Å and as weak with $\lambda = 0.8$ Å, or vice versa, thus allowing us to exclude fake reflections produced by the very low temperature experimental environment. The $NdVO_4$ single crystal was a needle of $0.5 \times 0.5 \times 4$ mm^3, oriented in the same way as $GdVO_4$. In this case, only the relatively longer wavelength $\lambda = 0.8395$ Å was used, since there were no issues with the absorption.

For both compounds some additional reflections were found below T_N, which are forbidden for conventional nuclear diffraction, indicating an antiferromagnetic spin configuration. A systematic search for satellites in the high-symmetry directions (q scans) of the reciprocal space gave no results with fractional wave vector $\mathbf{k}$. Therefore, $\mathbf{k} = 0$ was assumed for the spin configuration of both compounds.

B. Symmetry analysis

The possible magnetic symmetries have been analyzed in the frame of Bertaut's theory of spin configurations [30]. As discussed below, the crystal symmetry is zircon-type ($ZrSiO_4$-type), space group (s.g.) $I4_1/amd$, no. 141 in the ITC, with $Z = 4$ chemical units per cell. In the setting 1 of the ITC for this s.g., Gd atoms are located at the 4a sites Gd1 (0,0,0), Gd2 (0,1/2,1/4), Gd3 (1/2,1/2,1/2), and Gd4 (1/2,0,3/4). V is at the 4b site and O at a 16h site, $(0,y,z)$ with $y = 0.069(3)$, $z = 0.179(7)$, as refined at 8 K, in paramagnetic phase. For $NdVO_4$ the crystal structure is of the same type, with similar y and z parameters, which do not affect the discussion of the magnetic symmetry.

Let us consider first the combinations of the four spins $\mathbf{F} = \mathbf{s}_1 + \mathbf{s}_2 + \mathbf{s}_3 + \mathbf{s}_4$, $\mathbf{G} = \mathbf{s}_1 - \mathbf{s}_2 + \mathbf{s}_3 - \mathbf{s}_4$, $\mathbf{A} = \mathbf{s}_1 + \mathbf{s}_2 - \mathbf{s}_3 - \mathbf{s}_4$, and $\mathbf{C} = \mathbf{s}_1 - \mathbf{s}_2 - \mathbf{s}_3 + \mathbf{s}_4$. The full space group is generated (in addition to the integer translations) by the pure translation $t = (1/2,1/2,1/2)$ and the symmetry elements 1, 2_x, 2_y, 4_{1z}, and $\bar{1}$, respectively, identity, two-fold axes parallel to **a** and **b**, a four-fold screw axis parallel to **c**, and the space inversion. If 4_{1z} did not exist, but simply $2_{1z} = (4_{1z})^2$, the symmetry would be orthorhombic, s.g. $Imma$. Under this lower symmetry, any component of the cited combinations, F, G, A, and C, forms a one-dimensional irreducible representation. The 4_{1z} symmetry operation mixes some x and y components. Table I lists the actions of the symmetry elements on the F, G, A, and C combinations of each component of the spins. When considering 4_{1z}, the z components still make four single-dimensional representations. $A_{x,y}$ and $C_{x,y}$ give also rise to the one-dimensional representations $A_x \pm C_y$ and $A_y \pm C_x$. Each of these representations corresponds to a noncollinear antiferromagnetic configuration with equal x and y components. Finally, the action of 4_{1z} on $F_{x,y}$ and

TABLE I. Transformation of the spins under the symmetry operations of the space group $I4_1/amd$ for $\mathbf{k} = (0,0,0)$. The atom 1 is at $(x,y,z) = (0,0,0)$. Atoms 2, 3, and 4 are obtained by the symmetry operations $2_x = x, 1/2 - y, 1/4 - z$; $2_{1z} = 1/2 - x, 1/2 - y, 1/2 + z$; and $2_y = 1/2 - x, y, 3/4 - z$, respectively, also drawn in Fig. 5. The given combinations follow conventions similar to those of Bertaut [30]: $\mathbf{F} = \mathbf{s_1} + \mathbf{s_2} + \mathbf{s_3} + \mathbf{s_4}$, $\mathbf{G} = \mathbf{s_1} - \mathbf{s_2} + \mathbf{s_3} - \mathbf{s_4}$, $\mathbf{A} = \mathbf{s_1} + \mathbf{s_2} - \mathbf{s_3} - \mathbf{s_4}$, and $\mathbf{C} = \mathbf{s_1} - \mathbf{s_2} - \mathbf{s_3} + \mathbf{s_4}$.

	1	2_x	2_y	2_{1z}	4_{1z}	$\bar{1}$	t
F_z	F_z	$-F_z$	$-F_z$	F_z	F_z	F_z	F_z
G_z	G_z	G_z	G_z	G_z	$-G_z$	G_z	G_z
A_z	A_z	$-A_z$	A_z	$-A_z$	$-A_z$	$-A_z$	$-A_z$
C_z	C_z	C_z	$-C_z$	$-C_z$	C_z	$-C_z$	$-C_z$
A_x	A_x	A_x	A_x	A_x	$-C_y$	$-A_x$	$-A_x$
C_y	C_y	C_y	C_y	C_y	$-A_x$	$-C_y$	$-C_y$
A_y	A_y	$-A_y$	$-A_y$	A_y	C_x	$-A_y$	$-A_y$
C_x	C_x	$-C_x$	$-C_x$	C_x	A_y	$-C_x$	$-C_x$
F_x	F_x	F_x	$-F_x$	$-F_x$	F_y	F_x	F_x
F_y	F_y	$-F_y$	F_y	$-F_y$	$-F_x$	F_y	F_y
G_x	G_x	$-G_x$	G_x	$-G_x$	G_y	G_x	G_x
G_y	G_y	G_y	$-G_y$	$-G_y$	G_x	G_y	G_y

$G_{x,y}$ is to combine F_x with F_y and G_x with G_y, leading to two-dimensional representations for both cases. This classifies the 12 independent components s_{1i}, s_{2i}, s_{3i}, and s_{4i}, $i = x,y,z$, in a total of 10 irreducible representations, 8 one-dimensional and 2 two-dimensional. When considering the space inversion, one half of the representations are *gerade* (symmetric, the spatial inversion does not change the spin, but it does change the position of the spin) and one half *ungerade* (antisymmetric). Namely, F and G combinations are *gerade*, while and A and C are *ungerade*.

C. Data analysis

1. Magnetic structure of $GdVO_4$

For $GdVO_4$, we collected 103 reflections (30 unique) in the space group $I4_1/amd$ as a test, by using the four-circle geometry at room temperature. The observed set of intensities agreed with the nuclear structure that was obtained by x-ray diffraction (XRD) [31,32], namely, zircon-type. The allowed nuclear reflections (h,k,l) obey the s.g. conditions for (h,k,l), $h + k + l = 2n$; for (h,h,l), $2h + l = 4n$; and for $(h,\bar{h},0)$, $h = 2n$. The average internal consistency of equivalent reflections was $R_{w,\mathrm{int}} = 25\%$ over the intensities, which is similar to the agreement factor with the reported structural model, $R_w = 27\%$, $\chi^2 = 1.06$.

For $T = 90$ mK, all accessible reflections (h,k,l) with integer indexes were scanned, without any prior assumption about the space or magnetic group, i.e., assuming $P1$. We found additional reflections that are forbidden for the nuclear diffraction. The most intense ones are $(\pm1,\pm1,0)$, $(\pm3,\pm1,0)$, and $(\pm1,\pm3,0)$. For unpolarized neutrons, their intensity should be proportional to the squared modulus of the magnetic structure factor

$$\begin{aligned} F^m_{hkl} &= \alpha f_m(q)\mu_\perp\{\epsilon_1 + \epsilon_2 \exp[\pi i(k + l/2)] + \epsilon_3 \exp[\pi i(h + k + l)] + \epsilon_4 \exp[\pi i(h + 3l/2)]\} \\ &= \alpha f_m(q)\mu_\perp\{\epsilon_1 + \epsilon_3 \exp[\pi i(h + k + l)] + \exp[\pi i(k + l/2)]\langle\epsilon_2 + \epsilon_4 \exp[\pi i(h + k + l)]\rangle\}, \end{aligned} \tag{7}$$

where $\alpha = 2.695 \times 10^{-13}$ cm$/\mu_B$ is the magnetic scattering length, μ_B the Bohr magneton, $f_m(q)$ the form factor for Gd^{3+}, and $\mu_\perp$ the projection of the magnetic moment on the plane perpendicular to the scattering vector $\mathbf{q}$, and the sum runs over the four Gd atoms of the unit cell.

The ϵ_j factors are $\epsilon_j = 1$ for F modes, $\epsilon_1 = -\epsilon_2 = \epsilon_3 = -\epsilon_4 = 1$ for G modes, $\epsilon_1 = \epsilon_2 = -\epsilon_3 = -\epsilon_4 = 1$ for A modes, and $\epsilon_1 = -\epsilon_2 = -\epsilon_3 = \epsilon_4 = 1$ for C modes. Therefore, a magnetic ordering in each mode produces a type of systematic absences. For each mode, the intensity is zero if at least one of the following conditions is fulfilled:

F: $h+k+l = 2n + 1$, $2k + l = 4n + 2$, $2h + l = 4n + 2$,
G: $h + k + l = 2n + 1$, $2k + l = 4n$, $2h + l = 4n$,
A: $h + k + l = 2n$, $2k + l = 4n + 2$, $2h + l = 4n + 2$,
C: $h + k + l = 2n$, $2k + l = 4n$, $2h + l = 4n$,

where n is any integer.

Note that A and C modes would produce reflections with $h + k + l = 2n + 1$ but none of those have been observed. Thus, we either discard these modes, or we assume that the intensity is beyond observable. F modes would increase the intensity of the nuclear reflections. The reflection (2,2,0) has very small nuclear intensity. However, at 90 mK (2,2,0) should be intense due to the magnetic diffraction if the ordering was in any of the F_x, F_y, or F_z modes, in disagreement with observations. So, we discard F modes. Lastly, all of the observed non-nuclear reflections fulfill the aforementioned conditions for G modes, leading us to conclude that the ordering is a G mode.

Considering the direction of the moments, there are a few possibilities that need to be discussed, because only reflections with $\mathbf{q}$ very near the a^*b^* reciprocal plane can be scanned. The best fit to the experimental data was found for G_z. For this mode, all $(h,k,0)$-type reflections have the same $\mu_\perp = \mu$ and the intensities are different due to the form factor only. The most intense reflections would be the equivalent $(\pm1,\pm1,0)$ reflections with maximum form factor, and $|F^m_{\pm1,\pm1,0}| = |4\alpha f_m(q)\mu|$, with $\epsilon_1 = -\epsilon_2 = \epsilon_3 = -\epsilon_4 = 1$. The complete set of data has been analyzed with the FULLPROF suite of software [33] in the single-crystal mode. A fair agreement is observed for other magnetic reflections as depicted in a plot of observed-calculated squared structure factors (Fig. 4). The refined moment of Gd is $\mu = 7.2(3)\mu_B$ for $\lambda = 0.5$ Å and $\mu = 6.8(3)\mu_B$ for $\lambda = 0.8$ Å, both fully consistent with the expected value of $\mu = 7\mu_B$, corresponding to a spin-only atom with $L = 0$ and $J = s = 7/2$, where s is the spin, as in Gd^{3+}, and also in perfect agreement with the total magnetic entropy $S_m = R\ln(2s + 1)$. Details of the refinement can be found in the Supplemental Material [26].

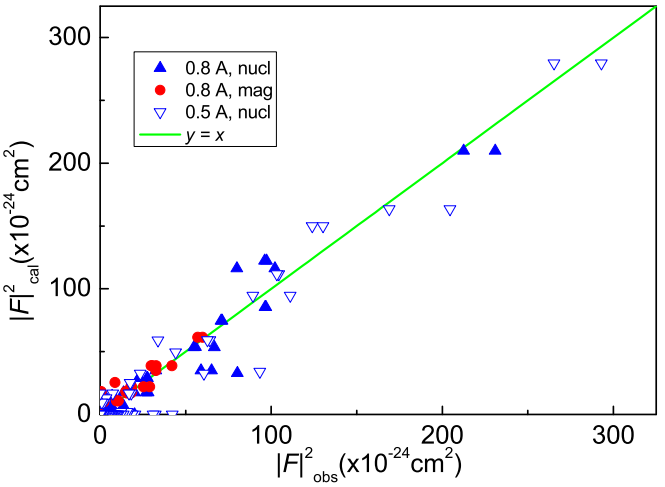

FIG. 4. Calculated vs observed squared structure factors for $GdVO_4$ at $T = 90$ mK. Red circles: Magnetic reflections. Triangles: Nuclear reflections, collected with $\lambda = 0.5$ Å and $\lambda = 0.8$ Å, as labeled.

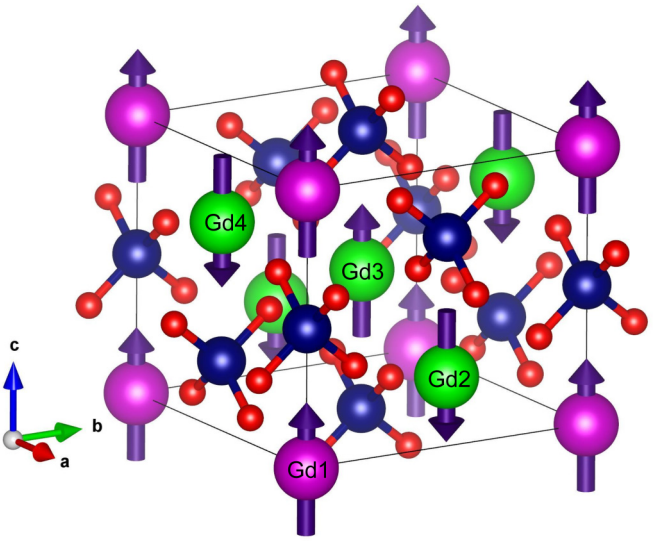

FIG. 5. Crystal and magnetic structure of $GdVO_4$ at $T = 90$ mK, from neutron diffraction. Red: O, blue: V, pink: Gd, green: Gd at (1/2,1/2,1/2) and its four nearest neighbors. The base atoms to obtain the magnetic irreducible representations in Table I are labeled as Gd1,..., Gd4. This structure corresponds to the G_z mode or the magnetic group $I4'_1/a'm'd$.

Let us consider now the G_x or G_y modes to discard these possibilities. These modes form a two-dimensional irreducible representation. According to Landau theory, for the present crystal symmetry the lowest free energy should occur with the moment of Gd1 aligned along the a or b axes, or along one main diagonal of the ab plane. In the first case, $|F^m_{\pm1,\pm1,0}|^2_{\rm cal}$ would be one half of the observed value for a moment of $7\mu_B$, or the refined moment would be $\sqrt{2} \times 7\mu_B$ to fit the observed intensity. In the second case, (1,1,0) would not be equivalent to $(-1,1,0)$, one of them being absent, but the intensity is the same within the experimental precision. Even in the case of a domain decomposition in such a small crystal, the average intensity of the set $(\pm1,\pm1,0)$ would be one half of the one observed. Therefore, the G_z mode not only fits the experiments better, but also is the only possible mode from physical considerations. The inclusion of small x, y components with other magnetic modes, does not improve the fit. We conclude that the simplest and best magnetic configuration, compatible with the observations, is the collinear antiferromagnetic G_z, in which each magnetic moment is antiparallel to its four nearest neighbors.

Figure 4 shows the agreement between the observed and calculated squared moduli of the structure factors. Since most reflections have both nuclear and magnetic contributions, we label each reflection as "magnetic" or "nuclear," according to its highest contribution. There are some experimentally weak reflections, which are not symetry allowed neither for the nuclear nor for the magnetic structure, that we label as "nuclear." Furthermore, there are no reflections with a high calculated $|F_{hkl}|$ and actually scanned but unobserved (i.e., at the y axis in Fig. 4). The largest discrepant reflections have been "observed" with only one wavelength, they show $|F_{hkl}|_{\rm obs} >> |F_{hkl}|_{\rm cal}$ and are attributed to spurious scattered neutrons by the low-temperature environment. In any case, the scattering length of Gd changes with λ and the nuclear structure factors do not need to be the same for both wavelengths. The resulting nuclear and magnetic structures are shown in Fig. 5, where one can see that the Gd atoms form a distorted diamond-type sublattice, with four nearest neighbors, indicated by green spheres.

2. *Magnetic structure of* $NdVO_4$

Based on heat capacity and magnetic susceptibility measurements, it was reported that $NdVO_4$ orders at $T_N = 820$ mK in an undetermined antiferromagnetic mode, with moments parallel to the c axis [16]. A peak in the ac susceptibility was reported to occur at T_N for the orientation parallel to the a axis, which was ascribed to a weak ferromagnetism.

The nuclear structure of $NdVO_4$ was tested at $T = 1.1$ K, in the paramagnetic state and with the same experimental conditions at lower temperatures (see below). The observed unit cell (i.e., zircon-type, with $a = 7.25$ Å, $c = 6.43$ Å) and intensities (Fig. 6) are perfectly compatible with the structure reported at room temperature from x-ray diffraction. [31]

Two collections of the intensities were performed in the magnetically ordered phase, at $T = 60$ and 500 mK, to observe the very probable change in intensity of the magnetic lines, due to the nuclear polarization of the ^{143}Nd and ^{145}Nd isotopes via the hyperfine field [21,22]. We have to consider that since T_N is not much higher than the range where the nuclear polarization takes place, both the electronic and nuclear contributions should be studied together. With respect to the reflections collected at 1.1 K, the new observed reflections at these lower temperatures are forbidden by the s.g. for the conventional nuclear diffraction and can be indexed as $(h,k,0)$, with $h,k = 2n + 1$. The q scans along high symmetry directions did not show any new reflection with fractional k. Therefore, the magnetic structure can be described by the wave vector $\mathbf{k} = 0$. Note that the observed magnetic reflections correspond to a G mode.

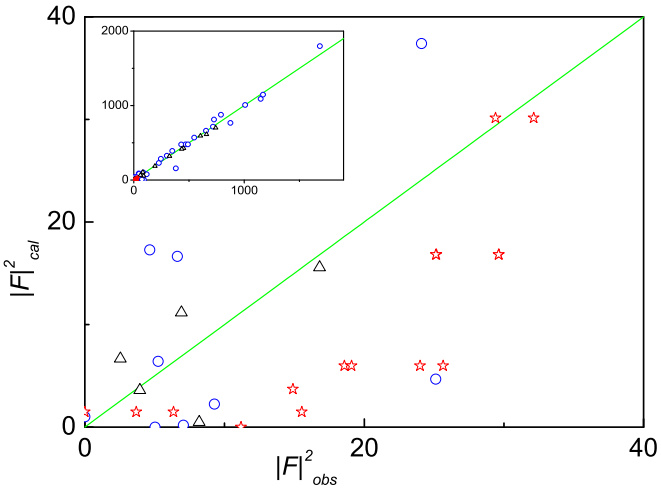

FIG. 6. Calculated vs observed squared structure factors for $NdVO_4$ at $T = 60$ mK and, for some of them, at 1.1 K. Triangles: A few conventional nuclear reflections scanned at 1.1 K. Circles: Reflections with the conventional nuclear contribution at 60 mK, computed only for nuclear scattering. Stars: Purely magnetic reflections. Straight line: Ideal agreement, $y = x$. Inset: All scanned reflections in a reduced scale, with the same symbol convention, giving some idea about the relative magnitude of the conventional nuclear scattering and the magnetic one, for Nd^{3+}.

To deduce the direction of the momenta from neutron diffraction is not a trivial task because of the following two experimental conditions. For now, only as an illustrative example (although confirmed *a posteriori*), let us consider the mode G_z. First, purely magnetic reflections of type $(0,0,l)$ with $l = 4n + 2$, e.g. (0,0,2), should be absent for this mode, since $\mu_\perp = 0$. The systematic absence of these type of reflections would determine unambiguously the z direction and the G_z magnetic mode. However, as in the case of $GdVO_4$, the normal beam geometry allows scanning only for $\mathbf{q}$ vectors near the a^*b^* reciprocal plane (also the ab direct plane for this s.g.) and the $(0,0,l)$ reflections are not accessible. Second, the nuclear polarization of Nd produces diffracted intensity for all reflections with the indexes allowed for any G mode, because the factor $\mu_\perp$ does not apply to this effect [see Eq. (8) below]. For instance, if the ordering mode was G_z and if the reflection (0,0,2) was accessible, its intensity should not be zero. There is not a temperature at which the magnetic order parameter is high and the nuclear polarization negligible, since the nuclear polarization occurs usually below 500 mK and there is no magnetic order at all above 820 mK. Therefore, the magnetic ordering and the nuclear polarization arise almost simultaneously on decreasing temperature.

Let us briefly consider the effect of the moment direction on the magnetic scattering. For a G_z magnetic ordering mode, all the reflections of the set $\{(\pm1,\pm1,0)\}$ are symmetry equivalent, as so are the sets $\{(\pm3,\pm1,0),(\pm1,\pm3,0)\}$ and $\{(\pm5,\pm1,0),(\pm1,\pm5,0)\}$. Moreover, the intensity ratio of two reflections of different sets is the squared ratio of the magnetic form factors of Nd^{3+}. For a G_x mode, $(\pm1,\pm3,0)$ should be nine times more intense than $(\pm3,\pm1,0)$ due to the different $\mu_\perp$ in the structure factor. Besides, $(\pm1,\pm5,0)$ would be 25 times more intense than $(\pm5,\pm1,0)$, and likewise for a G_y mode, exchanging the h and k indexes. Finally, for a G mode with the moments oriented along one of the two ab plane diagonals (let us call it G_{xy}), (1,1,0) and (1,−1,0) are not equivalent, since one of the two reflections should be absent, depending on the diagonal.

The experimental data at $T = 500$ mK give controversial results. We found that (1,3,0) is only 4 times more intense than (3,1,0), and (1,5,0) is only 2.5 times more intense than (5,1,0). The nonequivalency would support a G_x mode; however, the factors are much lower than expected. Moreover (1,1,0) and (1,−1,0) are not experimentally equivalent, but related by a factor of 3. On the other side, none of these last reflections is absent, hence, excluding a G_{xy} mode. A different approach would be to take the average intensity of the above three sets of reflections as a single observation. By doing so, the calculated data for G_x, G_y, or G_{xy} would give the same average, but for G_z they would exactly be twice as high. Fixing the scale factor from the nuclear diffraction, one model should fit better than the others. The intensity ratio of the reflections (1,1,0), (3,1,0), and (5,1,0) do not follow the squared form factors, the high q reflections being more intense than expected for purely magnetic scattering. This fact indicates a contribution of the nuclear polarization. If we were to neglect the nuclear polarization, data for the (1,1,0) set (the most intense due to the larger form factor, when the effect of the nuclear polarization would be relatively smaller) would fit fairly well for a moment $\mu = 0.9\mu_B$ and G_z mode. This value is consistent with the Curie-Weiss constant $C = 0.29$ emu K mol^{-1} Oe^{-1}, which corresponds to a paramagnetic moment of $\mu = 1.2\mu_B$ [17]. For a G mode in the ab plane, a value of $0.9\sqrt{2}\mu_B$ would be deduced. We considered a reflection as "observed" when the standard error on the integration of the profile is at most 1/4 of the intensity. So the most probable mode is G_z and the differences are simply due to experimental uncertainties. In addition to this, a G_z mode agrees with the single-crystal susceptibility data [16] suggesting that the moments lie along the c axis. Considering the small moment of Nd, less than 1 μ_B, weak ferromagnetic components F_x or F_y are far beyond the experimental limit to be directly observed by neutron diffraction experiments, when the intensity is superposed to the much stronger conventional nuclear diffraction (see in Fig. 6 a comparison of the nuclear and magnetic structure factors for the main magnetic contribution, G_z). Details of the conventional refinements and observed and calculated structure factors can be seen in the Supplemental Material [26].

3. *Nuclear polarization of Nd*

At $T = 60$ mK the magnetic reflections are still weak, though clearly observable. They also obey the extinction rules for a G mode. Figure 6 shows the calculated vs observed squared structure factors, using the fit of nuclear reflections to adjust the scale factor, and the usual expression for the magnetic structure factor, Eq. (7), as used by the FULLPROF software [33]. Note that some reflections labeled as "magnetic" are forbidden for the conventional nuclear scattering in this space group. These have been computed for a G_z mode and $\mu = 0.9\mu_B$. Reflections labeled as "nuclear" have been computed assuming a nonmagnetic nuclear structure (i.e., as at 1.1 K) and the conventional bound scattering lengths for each

atom. The nuclear reflections agree very well with the structure deduced at room temperature from x-ray diffraction. However, the magnetic reflections do not agree with any of the G_x, G_y, G_z, or G_{xy} modes. In particular $|F|_{\rm obs} > |F|_{\rm cal}$ for all the magnetic reflections, and the relative difference systematically increases for smaller $|F|_{\rm obs}$. In other words, there are clearly observed reflections that should be very weak (especially due to the small form factor for high q, which is independent of the ordering mode) indicating that the model of scattering by the magnetic moment of the electrons alone cannot explain the observed intensities.

At low temperatures, the ^{143}Nd and ^{145}Nd nuclei (ca. 20% of natural Nd) can be polarized by the hyperfine magnetic field produced by the unpaired electrons. For a nucleus with nuclear spin I, the incoherent scattering length (i.e., the nuclear spin incoherence, not the isotopic one) comes from the random relative orientation of the neutron and nuclear spins, viz., the bound scattering length depends on the total angular moment of the system $I + 1/2$ or $I - 1/2$. Normally, this value is at random in different sites, therefore leading to an incoherent scattering, similar to x-ray scattering when two different atoms randomly occupy the same crystallographic site. For a system of fully polarized nuclei, it is no longer at random, and $I + 1/2$ is selectively in some sites and $I - 1/2$ in others, whatever the neutron spin might be. If the polarization came from the electronic magnetic field, this effect would lead to a new coherent diffracted intensity, corresponding to the same spatial periodicity as that of the magnetic moments. The diffracted reflections obey the same extinction rules as the magnetic ones, but the form factor is 1, because the nucleus size is much smaller than the wavelength. This fact allows us to observe high-angle "magnetic" reflections. Besides, there is no $\mu_\perp$ term, this last one coming from the tensorial dipolar neutron-electron magnetic interaction. The nuclear polarization effect is strong for nuclei with large incoherent scattering lengths, like ^{143}Nd and ^{145}Nd, contrary to the magnetic neutron-nucleus interaction, which can be safely neglected in the case of thermal neutrons and typical nuclear moments near 1 nuclear magneton ($\simeq 1/2000\ \mu_B$).

When Nd is partially polarized, taking into account the fraction of polarizable isotopes and their experimental incoherent length, the magnetic plus hyperfine structure factor can be obtained by replacing the factor $\alpha f_m(q)\mu_\perp$ with $\alpha f_m(q)\mu_\perp + b_{\rm eff}\mu_N B_{hf}/(k_B T)$ in Eq. (7). We thus obtain

$$F^{m+h} = 4\left[\alpha f_m(q)\mu_\perp + b_{\rm eff}\frac{\mu_N B_{\rm hf}}{k_B T}\right], \qquad (8)$$

where $b_{\rm eff} = 0.133(18) \times 10^{-12}$ cm is determined by a weighted average of the incoherent scattering lengths of ^{143}Nd and ^{145}Nd [21,22]. $B_{\rm hf}$ is the hyperfine field acting on the Nd nucleus, and μ_N the nuclear magneton. The factor 4 accounts for the Nd atoms in the unit cell, when all the positional interference terms $\epsilon_j \exp[2\pi i(hx_j + ky_j + lz_j)] = 1$, $j = 1 - 4$, for the reflections of type $(h,k,0)$ with $h,k = 2n + 1$, allowed for the G mode. The last term is the high-temperature approximation of the Brillouin function, valid for $\mu_N B_{\rm hf}/k_B T \ll 1$ (a typical value for Nd is $B_{\rm hf} \simeq 100$ T, as computed from first principles in Ref. [22]).

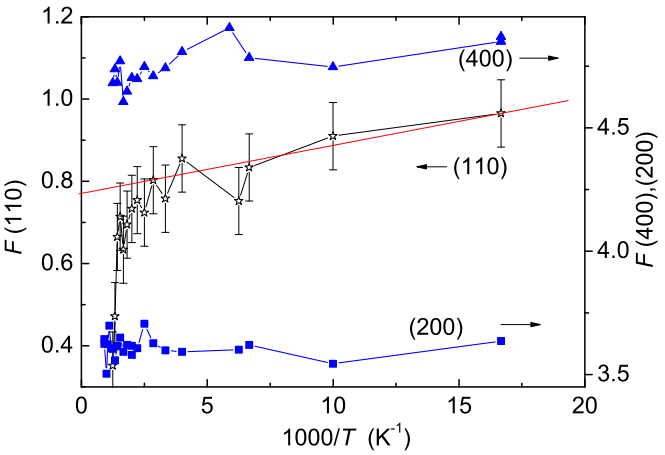

FIG. 7. Observed structure factors for the purely (conventional) nuclear reflections (2,0,0) and (4,0,0), right scale, along with the purely magnetic reflection (1,1,0), left scale. The scale factor has been deduced from the refinement of the nuclear structure.

The reflections (2,0,0), (4,0,0), and (1,1,0) have been scanned at several temperatures, starting from the lowest $T = 60$ mK. The scale factor to convert intensities to observed structure factors, $I_{hkl,\rm obs} = 37.42|F_{hkl}|^2_{\rm obs}(\times 10^{-24}{\rm cm}^2)$, has been deduced from refining the nuclear structure at 1.1 K. The observed structure factor of these reflections has been plotted as a function of $1/T$ in Fig. 7. The intensities of the purely nuclear reflections (2,0,0) and (4,0,0) remain nearly constant at any temperature, while the purely "magnetic" reflection (1,1,0) shows a dependence which is nearly linear at low temperatures and drops at $T_N = 820$ mK. Note that the linear dependence can be described by Eq. (8) when the electronic moment is saturated, which occurs for $T \ll T_N$, indeed. By taking a straight line as asymptote, the extrapolation to $1/T \to 0$ gives $4 f_m(q)\alpha\mu_\perp = 0.78 \times 10^{-12}$ cm, which corresponds to an electronic moment of $\mu = 0.8\mu_B$ assuming $f_m(q) = 0.926$ for the reflection (1,1,0) [29]. The so-obtained value of the electronic moment is somewhat lower than that deduced from susceptibility experiments. Also theory imposes lower and higher bounds for the Nd^{3+} (electron configuration: $[Xe]4f^3, {}^4I_{9/2}$) moment μ, when $1\ \mu_B \leqslant \mu \leqslant 3.27\ \mu_B$. The lower bound corresponds to a strong crystal field with a complete quenching of the orbital moment and the lowest total spin for the three $4f$ electrons, while the upper bound is the Landé rule for the free ion. A lower than expected μ value can be explained if some canting or weak ferromagnetism exists in modes F_x or F_y. However, its contribution to neutron diffraction should be very minor and superimposed onto the conventional nuclear diffraction, thus well beyond the experimental limit. Note that a moment of $1\mu_B$ is already difficult to observe even for an antiferromagnetic mode, as can be seen by, e.g., comparing the magnetic and nuclear scattering intensities in the inset of Fig. 6. Finally, we observe in Fig. 7 that the slope of the asymptote gives the hyperfine, $B_{\rm hf} = k_B/(4b_{\rm eff}\mu_N) = 55$ T, which is close to the value observed in $NdAlO_3$, $B_{\rm hf} = 66$ T, but below the theoretical calculation giving $B_{\rm hf}/\mu \simeq 113\ {\rm T}/\mu_B$ [22], or $B_{\rm hf} \simeq 90$ T for this compound.

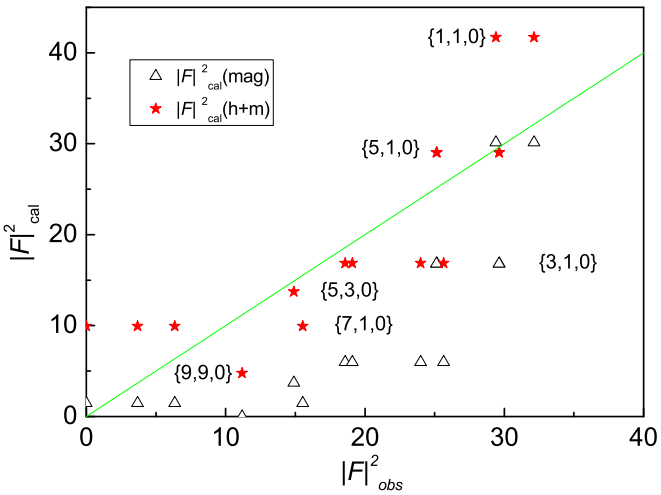

FIG. 8. Calculated vs observed squared structure factors of purely magnetic reflections for $NdVO_4$ at $T = 60$ mK and G_z mode. Triangles: Purely magnetic scattering computed for $\mu = 0.9\mu_B$. Stars: Magnetic and nuclear polarization, both included. Indexes in braces correspond to sets of equivalent reflections (all at the same horizontal line), as defined in the main text.

Figure 8 shows all the magnetic reflections scanned at $T = 60$ mK. Taking into account all reflections, together with the hyperfine and magnetic contributions, the experimental data have a fair agreement with $\mu = 0.8\mu_B$ and $B_{\rm hf} = 110$ T, that is, in much better agreement with the aforementioned theoretical calculation and previous data. The high-angle set of reflections (7,1,0) and (9,9,0) have nearly negligible magnetic intensities, due to the decay of the form factor. Still, they can be measured, although having an uncertainty that is roughly as large as their intensities.

V. DISCUSSION

The neutron diffraction data show that the Gd-Gd interaction in the zircon-type phase of $GdVO_4$ undoubtedly is antiferromagnetic, thus confirming the expected behavior supported by magnetic susceptibility and heat capacity data (e.g., the magnetic ordering peak remains up to field values as high as 1 T) [24,25]. This interaction explains the observed G-type magnetic ordering, as that of minimum energy, in which each ion is antiparallel to its four nearest neighbors. The spin-flop field should likely be larger than 1 T, even for this highly isotropic ion as Gd^{3+}. A spin-flop field of 1.08 T at 0.5 K and a transition to a paramagnetic state at 2.18 T is reported in Ref. [24]. The $\bar{4}m2$ symmetry of the Gd site requires one of the maximum or minimum anisotropy energy directions to be parallel to the crystal **c** axis and the other two parallel to **a** and **b**, or to the diagonals $\mathbf{a} \pm \mathbf{b}$, respectively. The dipolar interaction energy is relatively small and amounts to ca. -0.5 K, also favoring the G_z configuration. This fact is obvious from simple considerations and can also be verified in the isostructural $YbVO_4$, which has a very small exchange and orders at 93 mK in the G_z mode, with a magnetic moment of $\mu = 3.1\mu_B$, being that the dipolar energy scales with μ^2 [34].

One of the aims of our work is to analyze how the results for $GdVO_4$ compare with those for the isostructural $GdCrO_4$, this is, when Cr^{5+} replaces the nonmagnetic V^{5+}. For $GdCrO_4$, Gd^{3+} ions behave as a practically paramagnetic ensemble of $s = 7/2$ spins subjected to a much stronger exchange due to the Cr^{5+} ions, which order ferromagnetically at $T_C = 21$ K. [8] At temperatures much lower than T_C, the Cr^{5+} moments are nearly saturated, giving rise to an internal field that polarizes the Gd^{3+} ions in the same way as if there were an external field of ca. 7 T. The great advantage is that this field enhances the MCE, at relatively high temperature (i.e. $T >> 1$ K), which in combination with the high magnetic density makes this system interesting for applications. In $GdVO_4$, we have the opportunity to study the magnetic behavior of the same Gd sublattice, though without the influence exerted by the Cr internal field, viz., only with the presence of the measured applied field.

Concerning practical applications at low temperatures, $GdVO_4$ has been proposed as a good material for passive regenerators in GM cryocoolers, especially close to the liquid-helium boiling point, where high heat capacity materials are crucial [13]. $GdVO_4$ is a very interesting candidate also for another reason. Simulations of a combined GM cycle including magnetization and demagnetization steps have shown an increase of the cooling power by a factor of 1.5 for low fields (ca. 0.5 T) and using ErNi as the regenerator material [15]. The use of small fields, though not ideally optimal, is necessary because of the otherwise unwanted dissipation by eddy currents. In comparison to ErNi, $GdVO_4$ is an electrical insulator what allows applying much higher magnetic fields without dissipation. Moreover this compound has even better refrigerant capacity because of its broader MCE peak. The magnetocaloric effect of ErNi reaches relatively higher values of the magnetic entropy change ($-\Delta S_T \simeq 0.4$ J cm^{-3} K^{-1} for 5 T at 10 K), [15] but only for a narrow T range, decreasing sharply for other temperatures. As a comparison, for the same field, $GdVO_4$ reaches $-\Delta S_T \simeq 0.3$ J cm^{-3} K^{-1} at 3 K but still a reasonably high $-\Delta S_T = 0.16$ J cm^{-3} K^{-1} at 10 K.

A further reason for interest lies in the fact that in the paramagnetic phase of an antiferromagnet, the molecular field works in opposition to the external field, viz., it tends to orient the moments against the net polarization induced by the external field. Therefore, the entropy decrement upon the field application is smaller with respect to that of a pure paramagnet, proportionally to M^2 for $\mu_B B/k_B T \ll 1$. Then it comes as no surprise that zircon $GdVO_4$ in the PM phase has a lower MCE than monazite $GdPO_4$, which orders almost exclusively by dipolar interactions at a much lower temperature. Even though $GdPO_4$ is among the paramagnetic materials with the largest MCE to date, it is nearly useless as a passive regenerator in a GM cycle. This is because its very weak magnetic correlations become relevant only at sub-kelvin temperatures, resulting in very low values of the zero-field heat capacity at temperatures near the liquid helium boiling temperature, $C_{B=0}(4.3\ \text{K}) = 0.068\ R$. [10] The relatively stronger interactions that characterize $GdVO_4$ yield an overall smaller MCE, though still larger than the reference refrigerant GGG, together with a relevant high heat capacity, $C_{B=0}(4.4\ \text{K}) = 0.27R$. These features make $GdVO_4$ an ideal regenerator in a combined magnetocaloric-GM cycle, operating down to a low temperature of around 4.2 K.

VI. CONCLUDING REMARKS

In summary, the study of the magnetic structures of the zircons $GdVO_4$ and $NdVO_4$ prove that the direct *R*-*R* exchange interaction is antiferromagnetic in both, giving rise to a *G*-type ordering. The neutron diffraction pattern can be explained as a G_z mode in agreement with reported magnetic measurements. In $NdVO_4$, G_z is the main order mode but some canting could be present. In this last compound the nuclear polarization of ^{143}Nd and ^{145}Nd is observed along with the magnetic ordering below 500 mK. A relatively small z component of the hyperfine field of 55 T suggests also a possible canting.

$GdVO_4$ has high capacity and a strong magnetocaloric effect above 2.5 K and would be a good material for a helium cryocooler based on the Gifford-McMahon cycle, enhanced by a magnetic field. This is also the case of the very closely related $GdCrO_4$, where the Gd-Cr exchange acts as an effective polarizing field, producing high magnetocaloric effect over a wide temperature range, and high heat capacity even without any external field. The study of $GdVO_4$ physics gives valuable information for other isostructural compounds but this one also has interesting properties regarding technological applications at low temperatures.

ACKNOWLEDGMENTS

M.E. thanks the Donostia International Physics Center (DIPC) for the support of his stay in San Sebastián. This work has been funded by the Spanish Ministerio de Economía, Industria y Competitividad through Projects No. MAT2017-86019-R and No. MAT2015-68204-R, DGA Consolidated Group E100, and Comunidad de Madrid Project S2009/PPQ-1626. Authors would like to acknowledge the use of the Servicio General de Apoyo a la Investigación-SAI, Universidad de Zaragoza. The Institut Laue-Langevin in Grenoble(France) is acknowledged for beam time allocation (experiment code 5-41-793, doi:10.5291/ILL-DATA.5-41-793).

[1] A. M. Tishin and Y. I. Spichkin, *The Magnetocaloric Effect and its Applications* (IOP Publishing, Bristol, UK, 2003).
[2] P. Shirron, Cryogenics **62**, 129 (2014).
[3] V. Franco, J. S. Blázquez, J. J. Ipus, J. Y. Law, L. M. Moreno-Ramírez, and A. Conde, Prog. Mater. Sci. **93**, 112 (2018).
[4] P. Wikus, E. Canavan, S. T. Heine, K. Matsumoto, and T. Numazawa, Cryogenics **62**, 150 (2014).
[5] S. Jeong, in Proceedings of the 6th IIR/IIF International Conference on Magnetic Refrigeration, Victoria BC, Canada, 2014 (unpublished).
[6] K. Matsumoto, T. Kondo, S. Yoshioka, K. Kamiya, and T. Numazawa, J. Phys.: Conf. Series **150**, 12028 (2009).
[7] T. Numazawa, K. Kamiyaa, S. Yoshiokaa, H. Nakagome, and K. Matsumoto, AIP Conf. Proc. **985**, 1183 (2008).
[8] E. Palacios, C. Tomasi, R. Sáez-Puche, A. J. Dos santos-García, F. Fernández-Martínez, and R. Burriel, Phys. Rev. B **93**, 064420 (2016).
[9] E. Palacios, C. Tomasi, R. Sáez-Puche, A. J. Dos santos-García, F. Fernández-Martínez, and R. Burriel, Solid State Phenom. **257**, 139 (2017).
[10] E. Palacios, J. A. Rodríguez-Velamazán, M. Evangelisti, G. J. McIntyre, G. Lorusso, D. Visser, L. J. de Jongh, and L. A. Boatner, Phys. Rev. B **90**, 214423 (2014).
[11] B. Fisher, J. Hoffmann, H. G. Kahle, and W. Paul, J. Magn. Magn. Mater. **94**, 79 (1991).
[12] K. Dey, A. Indra, S. Majumdar, and S. Giri, J. Mater. Chem. C **5**, 1646 (2017).
[13] T. Numazawa, K. Kamiya, T. Satoh, H. Nozawa, and T. Yanagitani, IEEE Trans. Appl. Supercond. **14**, 1731 (2004).
[14] G. J. Bowden, Aust. J. Phys. **51**, 201 (1998).
[15] H. Yayama, Y. Hatta, Y. Makimoto, and A. Tomokiyo, Jpn. J. Appl. Phys. **39**, 4220 (2000).
[16] H. Suzuki, Y. Masuda, and M. Miyamoto, J. Phys. Soc. Jpn. **52**, 250 (1983).
[17] H. Suzuki, Y. Higashino, and T. Inoue, J. Phys. Soc. Jpn. **49**, 1187 (1980).
[18] R. I. Shermer, Phys. Rev. **130**, 1907 (1963).
[19] W. Marti, M. Medarde, S. Rosenkranz, P. Fischer, A. Furrer, and C. Klemenz, Phys. Rev. B **52**, 4275 (1995).
[20] I. Plaza, E. Palacios, J. Bartolome, S. Rosenkranz, C. Ritter, and A. Furrer, Physica B **234–236**, 635 (1997).
[21] J. Bartolomé, E. Palacios, M. D. Kuzmin, F. Bartolomé, I. Sosnowska, R. Przenioslo, R. Sonntag, and M. M. Lukina, Phys. Rev. B **55**, 11432 (1997).
[22] E. Palacios, J. Bartolomé, F. Luis, and R. Sonntag, Phys. Rev. B **68**, 224425 (2003).
[23] T. Chattopadhyay and K. Siemensmeyer, Europhys. Lett. **29**, 579 (1995).
[24] J. D. Cashion, A. H. Cooke, L. A. Hoel, D. M. Martin, and M. R. Wells, Proc. Colloq. Intern. CNBS Eléments Terres Rares **180**, 417 (1970).
[25] J. H. Colwell, B. W. Mangum, and D. D. Thornton, Phys. Rev. B **3**, 3855 (1971).
[26] See Supplemental Material at http://link.aps.org/supplemental/10.1103/PhysRevB.97.214401 for details of the nuclear and magnetic structure determinations.
[27] F. Pobell, *Matter and Methods at Low Temperatures* (Springer-Verlag, Berlin, 2007).
[28] H. Kimura, M. Sato, Y. Terada, K. Shimamura, T. Fukuda, and S. Miyashita, J. Mater. Sci. **33**, 2379 (1998).
[29] E. N. Maslen, in *International Tables for Crystallography*, Vol. C (Kluwer Academic Publishers, Dordrecht, The Netherlands, 1992), Table 6.3.3.2, p. 523.
[30] E. F. Bertaut, in *Magnetism*, Vol. 3, edited by G. T. Rado and H. Suhl (Academic, New York, 1963).
[31] W. O. Milligan and L. W. Vernon, J. Phys. Chem. **56**, 145 (1952).
[32] D. F. Mullica, E. L. Sappenfield, M. M. Abraham, B. C. Chakoumakos, and L. A. Boatner, Inorg. Chim. Acta **248**, 85 (1996).
[33] J. Rodríguez-Carvajal, Physica B **192**, 55 (1993); J. Rodríguez-Carvajal and T. Roisnel, Commission for Powder Diffraction Newsletter 20 (International Union for Crystallography, 1998), p. 35, https://www.ill.eu/sites/fullprof/.
[34] P. Radhakrishna, J. Hammann, and P. Pari, J. Magn. Magn. Mater. **23**, 254 (1981).